WIND TUNNEL SIMULATIONS OF THE ATMOSPHERIC BOUNDARY LAYER

by

KENNETH A. de CROOS

B.S.M.E., University of Notre Dame, 1974

A THESIS SUBMITTED IN PARTIAL FULFILMENT OF THE REQUIREMENTS FOR THE DEGREE OF MASTER OF APPLIED SCIENCE

in the Department of Mechanical Engineering

We accept this thesis as conforming to the required standard

THE UNIVERSITY OF BRITISH COLUMBIA

December, 1976

In presenting this thesis in partial fulfilment of the requirements for an advanced degree at the University of British Columbia, I agree that the Library shall make it freely available for reference and study. I further agree that permission for extensive copying of this thesis for scholarly purposes may be granted by the Head of my Department or by his representatives. It is understood that publication, in part or in whole, or the copying of this thesis for financial gain shall not be allowed without my written permission.

Kenneth A. de Croos

Department of Mechanical Engineering

The University of British Columbia,
Vancouver, Canada

Date 27 - 4 - 77

"Big whirls have little whirls that feed on their velocity,
Little whirls have lesser whirls, and so on to viscosity."

L.F. Richardson

ABSTRACT

The velocity profile shape and boundary layer thickness of an equilibrium boundary layer grown over a long fetch of roughness are closely matched with those of a boundary layer artificially thickened using spires (by adjusting the shape and height of the spires). Other turbulent characteristics of these two wind tunnel simulations of the atmospheric wind are then compared. At the same time, more information on rough wall boundary layers is obtained to allow for a rational choice of the shape and spacing of roughness elements required to produce a particular simulation of the full scale boundary layer.

A technique for calculating the shape of boundary layers in exact equilibrium with the roughness beneath, using a data correlation for the wall stress associated with very rough boundaries and a semi-empirical calculation method, is examined experimentally. Wall shear stress, measured directly from a drag plate, is combined with boundary layer integral properties to show that the shear stress formula is reasonably accurate and that the boundary layer grown over a long fetch of roughness is close to equilibrium after passing over a streamwise distance equal to about 350 times the roughness element height.

The boundary layer quickly generated using spires proved to be a fair approximation to that grown over a long fetch of roughness, but did not accurately represent the longitudinal turbulence intensity of the full scale atmospheric wind or the naturally grown boundary layer.

The boundary layer produced here by spires showed little change in gross characteristics after travelling about eight spire heights downstream of the spires. A distance of six or seven such heights has been advised by other workers in the past.

ACKNOWLEDGEMENTS

The author wishes to express his sincere appreciation and thanks to Dr. Ian Gartshore. Only his patient supervision and expert guidance made this work possible.

Thanks also for the invaluable assistance and encouragement rendered by Ashok Malhotra with the initial analytical considerations, and Rick Edey with the experimental work.

This research was funded under National Research Council of Canada Grant A-4308.

TABLE OF CONTENTS

LIST OF TABLES

LIST OF FIGURES

Figure Page

NOMENCLATURE

A, A_1, B_1, C	constants
A_F	frontal area of one roughness element
A_P	effective floor plan area associated with each roughness element
C_{D_B}	drag coefficient of a square bar
C_{D_R}	drag coefficient of one roughness element
e	slant wire rms voltage
E	slant wire mean voltage
H	shape factor = δ^*/θ
H_1	unusual shape factor $\equiv \frac{\delta - \delta^*}{\theta}$
K	von Karman's constant
x_{Lu}	integral length scale
k	roughness element height
k_1	a constant depending on the aspect ratio of a hot wire
n	frequency, cps
Re	Reynolds number
$S_{uu}(n)$	power spectrum ft^2/sec
Tu	integral time scale
U	local mean velocity, ft/sec
U_1	free stream velocity or gradient wind, ft/sec
U_τ	friction velocity, = $\sqrt{\frac{\tau_0}{\rho}}$

u	$= \sqrt{\overline{u^2}}$ rms of the turbulence velocity in the x-direction, ft/sec
x	streamwise distance; distance downstream
z	height above ground
z_0	roughness length, $z = z_0$ at $U = 0$
α	shape factor, $= \frac{H-1}{2}$; power law exponent if a power law is assumed
δ	boundary layer thickness
δ^*	displacement thickness
λ	bar spacing; distance between square roughness bars
λ_e	"equivalent" bar spacing
ρ	air density
θ	momentum thickness
ψ	angle of yaw, usually 45° for a slant wire
τ	shear stress
τ_0	surface shear stress
ν	kinematic viscosity

CHAPTER 1

INTRODUCTION

The atmospheric wind has always had a strong effect on man and his environment. Within the last fifteen years or so, an overall concern for human comfort and safety has led to a need for more extensive data on wind characteristics in the atmospheric boundary layer. Reasons for renewed engineering interest in the study of wind effects include economic loss, and loss of life and limb caused by wind devastation, problems that could grow alarmingly with urban concentration and population increases.

Engineers need to obtain more data on forces on glass and cladding in tall structures, as well as the deflections of the structures themselves, caused by the atmospheric wind. Another concern is human comfort in pedestrian areas surrounded by tall structures, and in the upper regions of these structures. Also wind-induced oscillations of bridges and transmission lines have to be predicted. The need to control air pollution has caused interest in the dispersive properties of the atmospheric boundary layer. Wind effects on nuclear power plant structures and large solar collectors must be considered when developing alternative energy sources.

Theoretical methods used to predict these flow processes would involve a combination of meteorology, fluid mechanics, and structural mechanics, and at present require drastic assumptions and simplifications. An increasingly common and very effective method of obtaining data on wind effects on full scale systems is to test small scale models in a reasonable simulation of the lower portion of the neutral atmospheric boundary layer. Under strong wind conditions, the intense turbulent mixing in the wind leads to an adiabatic lapse rate, so that a model boundary layer with isothermal conditions is suitable for these studies.

Various methods are used to obtain a satisfactory model of this neutral atmospheric boundary layer. One technique is to grow the boundary layer over a long fetch of roughness elements upstream of the test model, as advocated by Davenport[1] and Cermak.[2] The dimensions of each roughness element and the roughness spacing geometry can be altered to produce the required velocity profile shape. This long fetch of roughness elements is then representative of the full scale roughness (trees, buildings, etc.) that the atmospheric boundary layer grows over. The disadvantage with this method is that it requires a large wind tunnel with a working section about 80 ft long in order to produce a boundary layer 2 to 4 feet thick.

When it is necessary to produce a boundary layer within a very much shorter distance, various techniques are used to thicken the boundary layer artificially and shape it to the desired velocity profile. One method is to use a set of mechanical devices, such as spires or wedges located at the entrance to the working section of the tunnel.[3,4] These devices, usually about as tall as the desired boundary layer thickness, vary in design and shape. Others prefer to use jets with air injection perpendicular to the flow,[5] or upstream oriented wall jets,[6] or a combination of jets with grids.[7]

Campbell and Standen,[8] in an exhaustive study using spires, grids and bars of various dimensions and combinations, found that trips could be designed for reasonable simulation of most of the turbulent characteristics of the atmospheric boundary layer. However, these characteristics were not all simultaneously simulated by one particular device or set of devices. For example, they found that a certain set of spires produced good simulation of the full scale velocity profile and turbulence intensity, but that the simulation of the atmospheric power spectrum was poor. A combination of short spires and a uniform mesh grid produced good power spectra, but other characteristics were not properly simulated. The general consensus of opinion appears to be that a

complete simulation of the atmospheric wind in all respects is difficult, and a compromise must be achieved whereby it is decided beforehand what aspects of the natural wind need be accurately represented, and a trip designed for these purposes.

If a thick turbulent boundary layer is grown over a long fetch of roughened floor, various methods have been used to scale this model boundary layer with the particular portion of the atmospheric boundary layer that is being simulated. In most instances, the geometry of the roughness elements on the floor has been chosen by trial and error. The shape of the velocity profile which must be produced by these elements is known in broad terms, however. Davenport[9] gives an indication of the values of the exponent α, for a particular terrain, if a power law of the form

$$\frac{U}{U_1} = \left(\frac{z}{\delta} \right)^{\alpha} \qquad \ldots (1)$$

is assumed.

Here U = local velocity

U_1 = free stream velocity or gradient wind

z = height above ground

δ = boundary layer thickness.

For example, Davenport suggests a power law exponent = 0.16 for open grassland, a value of $\alpha = 0.28$ for forest and suburban areas, and $\alpha = 0.40$ for city centres.

The objective of this work is to compare the characteristics of two boundary layers, one produced by a long fetch of roughness and the other by a set of spires. Identical measurements made under similar conditions would allow for a better comparison than would measurements made by different workers at separate facilities.

At the same time, more information on rough wall boundary layers is obtained to allow for a more rational choice of the shape and spacing of roughness elements. We first consider here theory on rough wall boundary layer approaches to equilibrium. The present experimental arrangements are then described, followed by a discussion of results obtained for both the long fetch of roughness and the shorter fetch with spires, known as the 'naturally grown' and 'artificially grown' cases respectively.

CHAPTER 2

ROUGH WALL BOUNDARY LAYERS

Prandtl[10] suggested that the fluid flow around objects, or over a flat plate, could be divided into two parts: (1) the boundary layer, often defined as the region in which the velocity of the fluid is less than 99 percent of the local maximum velocity of the flow (the free stream velocity), (2) the region outside this boundary layer, where there is usually no vorticity. The boundary layer is therefore the region in which almost all of the viscous losses occur. The velocity gradient is high, and the shear stresses are important. Outside the boundary layer, with little velocity variation, the resulting shear stresses are negligible. When the boundary is a flat plate, a laminar boundary layer is formed initially, with transition to a turbulent boundary layer occurring if the plate is long enough or if a small roughness element or "trip" is placed on the plate. The solution to the mathematical equations describing the laminar boundary layer is an infinite series, known as the Blasius solution. If the velocity profiles for a laminar boundary layer in zero pressure gradient are plotted in appropriate non-dimensional form, only one curve, the Blasius profile,

is obtained, regardless of the Reynolds number of the flow.

In turbulent flow, the time-averaged equations cannot provide a solution for the boundary layer velocity profile, and various semi-empirical profiles are used. One such velocity distribution has already been mentioned, the power law, derived from Blasius' resistance formula for smooth pipes, but also applicable to boundary layers in zero pressure gradient. If the non-dimensionalized velocity profiles for the smooth wall turbulent boundary layer are plotted, they do not collapse, as was the case with the laminar boundary layer, but instead form a family of profiles for varying Reynolds number. Clauser,[11] extending this idea to turbulent boundary layers on rough walls, shows that turbulent boundary layers form families of profiles dependent on both the Reynolds number and the degree of roughness on the wall.

Another semi-empirical profile is the so-called "law of the wall," derivable by dimensional analysis. For smooth walls, the mean velocity is expected to be of the form

$$\frac{U}{U_\tau} = f\left(\frac{z\,U_\tau}{\nu}\right)$$

which implies that a plot of $\left(\frac{z\,U_\tau}{\nu}\right)$ vs. $\left(\frac{U}{U_\tau}\right)$ for various flows will yield a single curve.

If, a small distance away from the wall, the velocity gradient $\frac{\partial U}{\partial z}$ is independent of the viscosity as well, then $(\frac{z}{U_\tau} \cdot \frac{\partial U}{\partial z})$ is a constant and the law of the wall can be written in the usual semi-logarithmic form:

$$\frac{U}{U_\tau} = \frac{1}{K} (\frac{z\, U_\tau}{\nu}) + A \quad ,$$

where K and A are constants, the former being called 'von Karman's constant'. Nikuradse[12] and others have verified that this law holds for both smooth and rough walls, even for moderate pressure gradients.

For fully rough walls,

$$(\frac{U_\tau k}{\nu} \geq 70) \quad ,$$

the viscosity is no longer important, and the law of the wall relationship becomes

$$\frac{U}{U_\tau} = f\,(\frac{z}{k})$$

(where k is a typical roughness height) provided that the region directly affected by individual roughness elements $(\frac{z}{k} \leq 2)$ and the region far from the wall $(\frac{z}{\delta} \geq \frac{1}{3})$ are excluded. Again, if, away from the immediate wall region we can take the velocity gradient $\frac{\partial U}{\partial z}$ to be determined by

U_τ and z only (not k), then $\frac{z}{U_\tau} \cdot \frac{\partial U}{\partial z}$ is a constant; and the semi-logarithmic relationship becomes

$$\frac{U}{U_\tau} = \frac{1}{K} \ell n(\frac{z}{k}) + B_1 \quad .$$

It can be assumed that the viscosity is not important for the outer, fully turbulent portion of the boundary layer; if the velocity defect (U_1-U) depends only on the shear stress at the wall, the boundary layer thickness and the distance z; then by dimensional analysis we have

$$\frac{(U_1-U)}{U_\tau} = g(\frac{z}{\delta}) \quad .$$

This is called the velocity defect law, which is satisfied experimentally for zero pressure gradient for the outer portion of the boundary layer, independent of wall roughness.

Clauser describes the turbulent boundary layer on a smooth wall in terms of an outer layer and an inner viscous sublayer next to the wall. By analogy, the rough wall boundary layer has an inner region which is dependent on the individual roughness elements, their shape, spacing and height. Outside this region, it appears that only

the effective wall stress affects the flow, the mechanism creating the shear stress (whether it be viscosity or surface roughness) being irrelevant.

The structure of the rough wall boundary layer therefore is as follows, and is shown in Figure I: (a) an inner "roughness" sublayer directly related to the roughness element geometry and shape, (b) a region extending from the top of this inner sublayer up to a height of about one-third the boundary layer thickness in which the law of the wall is applicable, (c) the outer region of the boundary layer, where the defect law is valid. Regions (b) and (c) may overlap, and the overlap region of the defect law would then be logarithmic.

Regions (a) and (b) are together sometimes called the constant stress layer. Although measurements in smooth wall boundary layers show that the shear stress is roughly constant for $z/\delta \leq 0.1$ (see Hinze[13] Section 7.7), the shear stress is not actually constant throughout regions (a) and (b). In rough wall boundary layers, the inner region (a) may be large enough to obscure any region of constant shear stress, as measurements by Antonia and Luxton[14] suggest.

Dvorak[15] made an extensive review of existing data obtained using square two-dimensional bar roughness

elements and used the form proposed by Clauser[16] to relate bar height (k) and spacing (λ) to the boundary layer displacement thickness (δ^*) and effective wall shear stress (τ_0) as follows:

$$\frac{U_1}{U_\tau} = \frac{1}{K} \ln\left(\frac{U_1}{U_\tau} \cdot \frac{\delta^*}{k}\right) + A - C \qquad \ldots . (2)$$

where

$$\left(\frac{U_\tau}{U_1}\right) = \sqrt{\frac{\tau_0}{\rho U_1^2}}$$

U_1 = free stream velocity--already defined in Equation (1).

ρ = density of fluid

A = constant ≈ 4.8

K = constant, usually taken to be 0.41

δ^* = displacement thickness, a measure of boundary layer height

and C is a constant depending on λ and k as follows:

$$C = 17.35 \left(.707 \ln \frac{\lambda}{k} - 1\right) \quad \text{for } \frac{\lambda}{k} \leq 4.68$$

$$C = -5.95 \left(.48 \ln \frac{\lambda}{k} - 1\right) \quad \text{for } \frac{\lambda}{k} \geq 4.68 \; . \qquad \ldots . (3)$$

From Equation (3), the value of C is a maximum when $\lambda/k = 4.68$. Closer bar spacing merely fills the tunnel, raising the effective floor height by producing greater mutual sheltering between the roughness bars.

The Equations (2) and (3) are strictly valid only for values of $\frac{U_\tau k}{\nu} \geq 70$, the "fully rough" condition, which is satisfied in most atmospheric applications. They allow the friction velocity ratio U_τ/U_1 to be obtained for any height ratio δ^*/k and spacing λ/k.

However, few rough boundaries can be approximated by the square two-dimensional bars used by Dvorak, and Gartshore[17] generalized the results to three-dimensional roughness elements of various shapes. This was done by defining an effective spacing between two-dimensional bars which produces surface drag per unit area (or average shear stress) equal to that of the three dimensional roughness pattern. From this work

$$\frac{\lambda_e}{k} = \frac{C_{D_B}}{C_{D_R}} \cdot \frac{A_P}{A_F}$$

where A_p is the effective plan area associated with each element, and A_F the frontal area.

The ratio λ_e/k is the equivalent spacing of two-dimensional bars of height k, which will produce wall

shear stress equal to that produced by the general roughness of height k. C_{D_B} and C_{D_R} are the drag coefficients of a bar and of one roughness element respectively measured under identical conditions. For square bars and cube shaped roughness with small upstream boundary layers (compared to roughness height),

$$C_{D_B} \simeq C_{D_R} \simeq 1.2 \qquad \text{(see references 18,19)}$$

and it is assumed here that for roughness elements whose frontal shape is nearly a square,

$$\frac{C_{D_B}}{C_{D_R}} \simeq 1 .$$

Therefore,

$$\frac{\lambda_e}{k} \simeq \frac{A_P}{A_F} . \qquad \ldots . (4)$$

Clearly, for random roughness, C_{D_R}, A_P and A_F would have to be statistical averages. So now λ_e/k from Equation (4) above can replace λ/k in Dvorak's relations and allow a generalization of his bar roughness correlation to any fully rough geometry. These relations are valid only for roughness provided by essentially isolated

roughness elements on comparatively smooth boundaries. Very close spacing between roughness elements would have a mutual sheltering effect similar to that from extremely closely spaced bar roughness, so that the restriction $\lambda_e/k > 5$ is placed on these relations.

In order to relate the velocity profile shape α to the friction velocity three equations are needed to solve for the unknowns U_τ, δ^* and α. Dvorak uses Equation (2) above as the first equation, and the momentum integral equation

$$\frac{\tau_0/\rho}{U_1^2} = \frac{d\theta}{dz} \qquad \ldots . (5)$$

(where θ is the momentum thickness related to δ^* and α) as the second equation. The third equation which he used is a standard empirical correlation known as Head's method. Empirically, Head devises functions F_1 and G_1 such that entrainment rate

$$\frac{d}{dx}\,[U_1(\delta - \delta^*)]$$

is related to the unusual shape factor

$$H_1 \equiv \frac{\delta - \delta^*}{\theta}$$

as follows:

$$\frac{1}{U_1}\frac{d}{dx}\left[U_1(\delta - \delta^*)\right] = F_1(H_1) \qquad \ldots\ldots(6)$$

where H_1 is related empirically to the usual shape factor $H \equiv \delta^*/\theta$ by

$$H_1 = G_1(H) \ .$$

The functions F_1 and G_1 are specified by the numerical description given in Appendix I.

The basis for these correlations is extensive work on smooth wall turbulent boundary layers, also valid for rough wall cases.[15]

For U_1 = constant (zero pressure gradient, Equation (6) above becomes

$$\frac{d}{dx}(\delta - \delta^*) = F_1(H_1) \ . \qquad \ldots\ldots(7)$$

Since H_1 is defined as $H_1 = \frac{\delta - \delta^*}{\theta}$, Equation (7) can be written as

$$\frac{d}{dx}(\theta H_1) = F_1(H_1) \ . \qquad \ldots\ldots(8)$$

Zero pressure gradient smooth wall boundary layers closely conform to the condition of exact equilibrium over

limited streamwise distances.[20] Equilibrium here means that the structure of the boundary layer does not change significantly in the streamwise direction, i.e., properties such as nondimensional spectra, turbulence intensities, etc., remain the same with changes in streamwise distance x. Exact equilibrium, also known as self-preservation,[21] is only possible for zero pressure gradient rough wall boundary layers in rather extreme cases: either the roughness elements are high compared to their spacing[22] or else the roughness height and spacing change with streamwise distance x such that they remain a constant fraction of the boundary layer thickness.[23]

Zero pressure gradient boundary layers developing over a constant roughness geometry with $\lambda_e/k \geq 5$ conform approximately to the condition of equilibrium after travelling a fairly long distance downstream of their origins. Estimates of this distance vary from 320 times the roughness height[24] to 1000 times the roughness height.[25] What this means is that boundary layer characteristics such as H, H_1 and α are not changing significantly with change in the streamwise distance x. In this case, the differential Equations (5) and (8) become arithmetic. For equilibrium, Equation (8) becomes

$$H_1 \frac{d\theta}{dx} = F_1 (H_1)$$

or,

$$\frac{d\theta}{dx} = \frac{F_1 (H_1)}{H_1} .$$

Since

$$H_1 = G_1 (H) ,$$

$$\frac{d\theta}{dx} = \text{function } (H)$$

and $\frac{d\theta}{dx}$ is therefore a constant since H is a constant. Now we define a new shape factor $\alpha = (\frac{H-1}{2})$. This shape factor is equal to the exponent of the power law (Equation(1)) if a power law is assumed. If a power law is not a good description of the velocity profile, then α is simply a non-dimensional description of the boundary layer shape. Now, since

$$\alpha = \frac{(H - 1)}{2} ,$$

$$\frac{d\theta}{dx} = \text{function } (\alpha)$$

and by comparison with Equation (5) the result is:

$$\frac{U_\tau}{U_1} = \text{function } (\alpha) . \qquad \ldots . (9)$$

Equation (9) shows that $\frac{U_\tau}{U_1}$ is a constant for any one equilibrium case (i.e., one shape of boundary layer), which is strictly possible from Equations (2) and (3) only when λ_e/k and δ^*/k remain constant, as already mentioned. Using Equation (2), Equation (9) above can be written as

$$\alpha = f_n \left[\frac{\delta^*}{k}, \frac{\lambda_e}{k} \right] . \qquad \ldots . (10)$$

It must again be emphasized here that the shape factor α as used here is simply defined by

$$\alpha = \frac{H - 1}{2}$$

where

$$H = \frac{\delta^*}{\theta} . \qquad \ldots . (11)$$

Also, since

$$\frac{\delta^*}{k} = \frac{\delta}{k} \left(\frac{\alpha}{1 + \alpha} \right) \qquad \ldots . (12)$$

can be used to define a nominal boundary layer thickness δ, equal to the actual boundary layer thickness if a power law profile exists, Equation (10) can be written as

$$\alpha = fn \left[\frac{\delta}{k}, \frac{\lambda_e}{k} \right] . \qquad \ldots . (14)$$

Equation (14) above is valid only for conditions at or near equilibrium.

The ratio $U_1\delta^*/U_\tau\delta$ is related to the defect law, as pointed out by Clauser.[16] By definition,

$$\delta^* = \int_0^\delta (1 - \frac{U}{U_1})\, dz \quad . \qquad \ldots . (15)$$

If the displacement thickness as given in Equation (15) above is combined with the defect law, which is

$$\frac{U_1 - u}{U_\tau} = \text{fn } (z/\delta)$$

it is easily shown that:

$$\frac{\delta^*}{\delta} \cdot \frac{U_1}{U_\tau} = \int_0^1 \frac{U_1 - u}{U_\tau}\, d(z/\delta)$$

$$= \int_0^1 f\ (z/\delta)\ d(z/\delta)$$

$$= \text{constant.}$$

The present equilibrium calculations from Head's method give a value of this parameter $(U_1\delta^*/U_\tau\delta)$ between 3.80 and 3.99, compared to Clauser's experimental value of 3.60 for boundary layers developing over constant roughness.

Various methods have been used by other workers to measure the friction velocity ratio U_τ/U_1, related to the wall shear stress by

$$\frac{U_\tau}{U_1} = \sqrt{\frac{\tau_0}{\rho U_1^2}}$$

and three of these methods are described here:

1. Shear stress can be obtained directly if the drag on a section of the floor (a drag plate) is carefully measured.

2. Shear stress can be inferred if a log law of the form

$$\frac{U}{U_\tau} = \frac{1}{K} \ln \left(\frac{z}{k}\right) \quad \ldots . (16)$$

is assumed. This technique necessitates assuming some figure for the von Karman constant, usually taken to be 0.41, an assumption which appears to be at best a rough approximation. Wooding et al.[26] point out that this value of 0.41 was obtained for classic cylindrical roughness shapes. Using a wide range of data gathered using roughness elements of many shapes

and sizes, they deduce that the value of the von Karman constant may lie between 0.25 and 0.41, depending on the type of roughness. These values will be discussed in the light of new experimental data in Chapter 4.

3. Another method for measuring shear stress that appears to have particular merit is the slanted hot-wire anemometer technique used by Patel,[27] and described in Appendix II. Of course, the slant wire cannot be used very close to the floor because of the roughness elements, but the constant stress region already discussed is expected, and should suffice to give a clear indication of the value of the wall shear stress τ_0.

All three of these measurement techniques have been used here and the results from all of them will be discussed in Chapter 4.

CHAPTER 3

EXPERIMENTAL ARRANGEMENTS

The U.B.C. wind tunnel used to gather experimental data is an open circuit, blower type tunnel 8 ft wide and initially 5 ft 2 in high with a test section 80 ft long. The area contraction ratio (ratio of the area of the entrance to the contraction to that of the entrance to the working section) is 4:1. The test section roof can be adjusted to maintain ambient room pressure throughout the test section, implying zero pressure gradient along the tunnel. Pressure taps located at 8 ft intervals along the back wall of the tunnel were connected to a multitube manometer for this purpose.

For the "naturally grown" boundary layer, the floor of the working section of the tunnel was covered with uniformly spaced roughness element strips 1.5 in high, 0.75 in wide and 0.041 in thick, as shown in Figure II. The strips were placed 6 in. apart from each other in lines across the tunnel. The lines were also 6 in. apart from each other, and a staggered pattern was used as shown, so that no roughness element was directly behind another roughness element in the row ahead of it. This

yields a value of A_p/A_F of 32 for Equation (4), and the assumption that the drag coefficients are equal gives a value of $\lambda_e/k = 32$ from Equation (4).

For experimental convenience, measurements with different lengths of roughness fetch were made at a fixed point 12 ft upstream from the open end of the wind tunnel. Adding or subtracting roughness sections upstream of the fixed point of measurement then yielded the required roughness fetch.

Antonia and Luxton[14] also found that the disturbance introduced by the first roughness element had a significant effect on the flow downstream. In order to reduce the importance of this factor, and also to reduce the importance of any length of smooth floor upstream of the first roughness elements, a wedge as high as the roughness elements (1 1/2 in) was placed across the tunnel. This wedge, of 8 in chord and as wide as the tunnel, then created a two-dimensional ramp and then a backward facing step. This wedge is referred to in later discussion as the 'trip' following common use of the term.

Mean velocity and rms measurements were made using a linearized hot wire in conjunction with a DISA type 55D01 anemometer, a DISA type 55D10 linearizer, and a DISA type 55D25 auxilliary unit. A Krohn-Hite Model

335 low pass filter* was used to reduce electronic noise.

Drag measurements were made using a drag plate, a floating isolated section of rough floor, about 7' x 3', fastened to an accurate wind tunnel balance. The gap around the drag plate was carefully made as small as possible, but not so small as to affect the readings by causing contact at high wind speeds.

The method of Cowdrey[28] was followed for the spire design, with modifications as made by Campbell and Standen.[8] The spires were designed to produce a boundary layer at about eight spire heights downstream that would match the measured measured shape factor α and measured boundary layer thickness δ of the "naturally grown" boundary layer which had been observed 61.6 ft downstream of the trip.

It was decided to design a simple array of flat wooden spires using 1/4 in plywood, the advantage with this construction being that the spires could be made slightly oversized, and then small changes to their profile made until the required specifications were met downstream. Campbell and Standen found that the best velocity profile was generated by modified half-width spires--that is, with spire width equal to half the boundary layer thickness. Before modification of these spires, Cowdrey's design was followed by Campbell and Standen with the result that the

*Filter setting equals 20 kHz.

spires were very sharply spiked at the top. As a result, a boundary layer thickness five-sixths the height of the spires was obtained by these workers. Hence, one of the modifications made by Campbell and Standen was to construct the modified half-width spires taller than the required boundary layer thickness.

For the purposes of this program, the design of Cowdrey, with the modifications made by Campbell and Standen, was followed. Also a further modification was added here, because the present plywood spires could not be very sharply spiked. The spires were designed to produce the desired shape factor α and boundary layer thickness δ, and were then smoothly rounded off at a height equal to about $0.85\,\delta$, where the spire width was very small. The distinction between the actual spire height (about $0.85\,\delta$) and the design spire height (about $1.10\,\delta$) must be pointed out, and is illustrated in Figure III. Clearly, the boundary layer thickness downstream of the present spires would be larger than the actual spire height, in contrast to the results of Campbell and Standen.

A short fetch of the same roughness as was used in the case of the naturally grown boundary layer was placed downstream of the spires. Drag measurements were made as before, using the drag plate. Again, for experimental convenience, data was taken at a fixed point, and

measurements at different distances behind the spires were made by moving the spires up or down the tunnel, and adding or subtracting roughness sections behind them.

Thus, in the cases of both naturally grown and artificially grown boundary layers the measurements do not relate precisely to a single boundary layer, since upstream of each fetch of roughness of streamwise length x there is a variable length of smooth floor equal to the tunnel length minus x.

In both cases, auto-correlations of the longitudinal turbulence velocity at various heights above the floor were obtained at the distances downstream where the velocity profiles were matched, using a PAR Model 101 Correlation Function Computer in conjunction with the DISA instruments already mentioned. Fourier analysis of these functions were made using a PAR Model 102 Fourier Analyser. All of these correlations and Fourier analyses were found to be repeatable.

The Reynolds number at which these tests were made was of the order of 3×10^4, where $Re = \frac{U_1 k}{\nu}$.

CHAPTER 4

RESULTS

The Naturally Grown Boundary Layer

Drag measurements were made using the drag plate for a wide range of wind velocities, at various distances downstream of the trip. Drag readings were found to be sensitive to tunnel pressure gradient, which was set as accurately as possible to zero by adjusting the tunnel roof. Drag readings were found to be accurately proportional to the square of the free stream velocity, as expected, indicating that no Reynolds number effects were present. This is illustrated in Figure IV. For clarity, data points are shown on only one line. All other lines were as well described by the experimental points, and all values were found to be repeatable.

Values of δ^* and θ were obtained by integration from the measured mean velocity profiles, using the relations

$$\delta^* = \int_0^{\delta} \left(1 - \frac{U}{U_1}\right) dz \qquad \ldots . (15)$$

and

$$\theta = \int_0^{\delta} \left(1 - \frac{U}{U_1}\right) \frac{U}{U_1} dz \; . \qquad \ldots . (17)$$

α and δ were then deduced from δ^* and θ as described previously in Equations (11) and (12). The velocity distributions were not particularly well described by the relation in Equation (1), but the values of δ estimated directly from the velocity profiles were close to the values obtained by the more precise integral method. An example of the power law profile plotted in the form $\log(U/U_1)$ vs. $\log(z/\delta)$, so that α is deduced directly from the slope of the plot, is shown in Figure V.

Measured values of δ^* and U_τ/U_1 are plotted in Figure VI, along with Dvorak's correlation of Equation (2). The measured values in Figure VI agree with the trend of the theory, and indicate an effective value of λ_e/k of about 30, which is close to the geometrical value of 32 obtained by Equation (4) using the assumption that the drag coefficients are equal. Thus, there is some verification for Dvorak's shear stress correlation for two-dimensional bars and its extension to three-dimensional roughness elements.

In Figure VII, where the shape factor α is plotted against δ, the calculated curves assume equilibrium conditions, i.e., that the shape factor is not changing significantly in the streamwise direction. As can be seen, the measured values approach the expected equilibrium, and are well represented by the equilibrium curve of

λ_e = 30 for the two largest values of x/k, i.e., x/k = 396.8 and x/k = 492.8.

This trend towards equilibrium at large values of x/k is also represented by the change in the integral defect law parameter $U_1\delta^*/U_\tau\delta$, given in Table II. It is seen that values of this quantity decrease from a value of 4.26 at the smallest value of x/k to a value of 3.96 at x/k = 492.8. Assuming exact equilibrium, this value is 3.99 for λ_e/k = 30 and α = 0.26.

From these figures it can be concluded that Dvorak's correlation of shear stress with integral boundary layer properties and roughness geometry is a useful correlation of rough wall boundary layer characteristics. From Figure VII and the defect law parameter $U_1\delta^*/U_\tau\delta$ we conclude that this rough wall boundary layer approaches equilibrium at a value of x/k $\approx$ 350. This is in agreement with the value of x/k $\approx$ 320 obtained by Antonia and Luxton,[24] and suggests that equilibrium can be approached quite closely for x/k less than 1000, the value suggested by Counihan,[25] from an extrapolation of non-equilibrium data.

In addition to the drag plate method, shear stress on the floor can be inferred from the log law, as previously discussed in Chapter 2, with some uncertainty, as to what value must be assumed for the von Karman constant.

If the classical value of K = 0.41 is assumed in the equation

$$\frac{U}{U_\tau} = \frac{1}{K} \ell n \left(\frac{z}{k}\right) \quad \ldots . (16)$$

values of U_τ/U_1 were found from the velocity profiles which were much larger than those obtained directly by the drag plate method. Since this suggested that the value of K was too large, the values of U_τ/U_1 obtained by the drag plate method for the various distances downstream from the trip were substituted in Equation (16). This, together with plots of the mean velocity profile, yielded values between 0.33 and 0.38 for von Karman's constant, as shown in Table II.

Artificially Grown Boundary Layer

The naturally grown boundary layer apparently reaches equilibrium in these tests for $x/k \leq 400$. We now wish to compare this equilibrium boundary layer with one grown artificially, that is, using spires, and developed in a shorter length of wind tunnel. For this purpose spires were designed as described in Chapter 3 to produce a boundary layer at about eight design spire heights (h) downstream whose gross shape (α) and thickness (δ) were

the same as the corresponding values measured in the equilibrium naturally grown case at $x/k \approx 400$. Comparisons of wall stress and turbulent characteristics; i.e., intensities, length scales, spectra etc., could then be made between the two cases.

As before, drag measurements were made using the drag plate. Roof adjustments were carefully made to maintain ambient room pressure throughout the length of the tunnel. Once again, drag readings were found to be repeatable, and proportional to the square of the free stream velocity, indicating the absence of Reynolds number effects.

Velocity profiles were taken at various distances behind the spires, and as in the case of the naturally grown boundary layer, values of δ^* and θ were obtained by integration using Equations (15) and (17). Values of α and δ were then deduced from δ^* and θ using Equations (11) and (12), as before, and are plotted in Figure VIII.

The measured values in Figure VIII show that beyond a distance of eight design spire heights, the values of δ^*, θ and α remain roughly constant. With regard to the streamwise gradients in the flow, this distance appears preferable to the six spire heights commonly used, at least as far as the present spire

design is concerned. It is not clear from Figure VIII whether equilibrium has been reached at the point where a close match was attempted with the naturally grown equilibrium boundary layer. The measured value of the defect law parameter at this point is equal to 4.12, compared with the calculated equilibrium value of 3.99, and the value of 3.96 for the naturally grown boundary layer at $x/k \approx 400$.

Measured values of δ^*, α, δ and U_τ/U_1 for the artificially grown boundary layer are also plotted in Figures VI and VII for $x \approx 8$ design spire heights, the point where a match with the equilibrium naturally grown boundary layer was attempted. In Figure VI, a value of λ_e/k greater than 30, in fact, closer to 40 is suggested. In Figure VII, where the plotted curves were calculated using the assumption of equilibrium, the value of λ_e/k suggested is very close to 30. However, this is not significant, since the spires were designed to produce these very values of α and δ. Equilibrium cannot be assessed by the values in Figure VII alone since the shear stress relation plotted in Figure VI must also be valid for the equilibrium plots of Figure VII to be valid.

Comparison Between the Two Simulations and With Full Scale Conditions

The shear stress measurements in the air using the slant wire technique are shown in Figure IV for each case at the streamwise positions where α and δ were matched. The values of $\tau/\rho U_1^2$ in each case approach the value on the floor as calculated using the drag plate method. Neither of the two simulations exhibit a region of constant shear stress extending upwards from the floor. However, as shown by Hinze[13] the shear stress is constant only in the region $x/\delta < 0.1$, and no measurements were taken below $x/\delta \approx 0.1$ here.

The slant wire was also used to measure the shear stress at distances beyond eight design spire heights behind the spires, where δ^*, θ and α remain roughly constant. It was found that the single point shown on Figure VI is representative of the artificially grown boundary layer more than eight design spire heights downstream from the spires.

Auto-correlations of the longitudinal turbulence velocity from the two simulations were taken at heights (z) of 2k, 5.3k and 10k. Fourier analysis of these functions were also made. Power spectral densities of the longitudinal turbulence from the two simulations at each height plotted in the form

$$\frac{n\, S_{uu}(n)}{\overline{u^2}} \quad \text{vs.} \quad n \cdot Tu$$

are shown in Figures X to XII, along with the well known von Karman spectrum, of the form

$$\frac{n\, S_{uu}(n)}{\overline{u^2}} = \frac{4n \cdot Tu}{[1 + 70.7(n \cdot Tu)^2]^{5/6}}$$

where

n = frequency in Hz.

$S_{uu}(n)$ = power spectrum ft^2/sec

Tu = integral time scale $\approx \frac{x_{Lu}}{\overline{U}}$

where

x_{Lu} = integral length scale.

The integral time scale was found in the present measurements by integrating autocorrelations in the usual way.

Also shown are representative results of full scale measurements taken from references 30 and 31. The power spectrum of horizontal wind speed at a height of about 330 ft shown in Figure X was taken in 1955-56 at the 375 ft meteorological tower of the Brookhaven National Laboratory by piecing together various portions of the spectrum. The data analyzed ranged from 5-day average speeds covering almost a year to 2 sec average speeds

covering an hour. The value of the power law exponent α for this set of measurements is not given in reference 30, but Templin[32] in a later work, deduces that a value of $\alpha = 0.28$ is appropriate for this case.

The full scale data shown in Figure XI for Montreal was taken on a tower in the Botanical Gardens, on the upper level of Mount Royal, at a height of about 250 ft. In this case, a value of $\alpha = 0.28$ is quoted by Davenport.[31] It is seen that the peak of this Montreal data is very well defined and coincides closely with the peaks of both the theoretical and experimental curves although the scatter does not enable us to define a slope clearly.

Davenport[9] gives a typical atmospheric boundary layer thickness of 1300 ft for $\alpha = 0.28$, allowing us to estimate $z/\delta \approx 1/4$ for Brookhaven, and $z/\delta \approx 1/5$ for Montreal respectively.

Both naturally grown and artificially grown boundary layers are close to the theoretical curve, with both curves exhibiting similar slopes to that of the von Karman spectrum over a wide range of reduced frequency $n \cdot Tu$. The distribution of energy is therefore roughly correct for both measured cases.

The biggest difference found between the two simulations is shown in Figure XIII, the plot of longi-

tudinal turbulence intensity. From a maximum value close to the floor, the rms values for the naturally grown boundary layer decrease sharply with an increase in distance above the floor z, similar to the full scale boundary layer. For the artificially grown boundary layer, the values of rms do not change much up to a value of z equal to about $1/2\,\delta$, and this is not representative of full scale conditions.

One interesting point to notice in connection with the intensities measured in the artificially grown boundary layer, is that these values increase as x increases for fixed z over a fairly large range of z, roughly $z \geq 1/2\,\delta$. This is possibly due to the transport of turbulent energy by the large scale motions from the wall region, where turbulence energy is high, and being produced, to the outer region, where it is lower, and where production is also low. The activity of these large scales appears to be too great in the artificially grown case, insofar as the turbulence level in the outer part of this boundary layer is significantly higher than the naturally grown case.

The full scale atmospheric turbulence intensity was obtained from reference 18, using a value of $z_0 \approx 30$ cm, where z_0 is the surface roughness length, as suggested by Davenport[9] for $\alpha \approx 0.28$.

CHAPTER 5

CONCLUDING DISCUSSION

Major conclusions with brief discussion of each are listed below:

1. Dvorak's correlation, and its extension to include three-dimensional roughness elements appears to be a useful method for predicting a roughness geometry which will produce a desired wall shear stress or shape factor, once equilibrium has been reached. Many problems remain to be solved--for example, the actual boundary layer development is not predicted here. However, this is a step towards more rational wind tunnel simulation of the atmospheric boundary layer [for individual cases, as opposed to the general 'city centre' boundary layer ($\alpha = 0.40$) or 'urban fetch' ($\alpha = 0.28$) currently in common use (see also reference 19)].

2. The present naturally grown boundary layer is close to equilibrium after passing over uniform roughness a distance downstream equal to about 350 times the roughness height. The agreement with the value of

about 320 obtained by Antonia and Luxton raises the interesting point--Does the value of x/k needed to reach equilibrium depend significantly on λ/k or on δ/k at equilibrium, or does it depend on the dimensions of the trip, or has it a relatively universal value? More work needs to be done in this area, as well as in predicting the actual boundary layer thickness which will be obtained over any given streamwise length of roughness fetch. Non equilibrium calculations must be used here, and it remains to be seen whether Dvorak's correlation and Head's method are sufficiently accurate to predict boundary layer growth far from equilibrium conditions.

3. This boundary layer quickly generated by artificial means proved to be a fair approximation to that grown over a long fetch of roughness. Whenever possible it is advisable to use that produced by the long fetch, however, and in any case to allow as long a fetch as possible downstream of the spires for the boundary layer to reach streamwise stability.

4. The boundary layer produced here by spires showed little change in gross characteristics δ^*, θ and δ after travelling about eight design spire heights downstream of the spires. A distance of six or seven such heights has been advised by other workers in the past.

5. This set of spires did not accurately represent the longitudinal turbulence intensity of the full scale atmospheric wind. The author is in agreement with Campbell and Standen in that the three main turbulent characteristics of the boundary layer, i.e., the velocity profile (shape and thickness), the power spectrum, and the turbulence intensity, cannot all be acceptably simulated by the same mechanical device, if in addition a reasonable degree of streamwise stability and moderate simplicity in the design and construction of the spires is required.

REFERENCES

1. Davenport, A.G., and Isyumov, N., "The Application of the Boundary Layer Wind Tunnel to the Prediction of Wind Loading," Paper No. 7, Proceedings of the International Research Seminar, National Research Council, Vol. 1, Ottawa (September 1967), University of Toronto Press, (1968).

2. Cermak, J.E., "Laboratory Simulation of the Atmospheric Boundary Layer," AIAA Journal, Vol. 9, (September 1971).

3. Counihan, J., "An Improved Method of Simulating an Atmospheric Boundary Layer in a Wind Tunnel," Atmospheric Environment, Vol. 3, (March 1969).

4. Standen, N.M., "A Spire Array for Generating Thick Turbulent Shear Layers for Natural Wind Simulations in Wind Tunnels," Report LTR-LA-94, N.A.E., (1972).

5. Schon, J.P., and Mery, P., "A Preliminary Study of the Simulation of the Neutral Atmospheric Boundary Layer Using Air Injection in a Wind Tunnel," Atmospheric Environment, Vol. 5, No. 5, (May 1971).

6. Nagib, H.M., Morkovin, M.V., Yung, J.T., and Tanatichat, J., "On Modeling of Atmospheric Surface Layers by the Counter-Jet Technique," AIAA Journal, Vol. 14, No. 2, (February 1976).

7. Teunissen, H.W., "Simulation of the Planetary Boundary Layer in the Multiple Jet Wind Tunnel," UTIAS Report 182, (June 1972).

8. Campbell, G.S., and Standen, N.M., "Progress Report II on Simulation of Earth's Surface Winds by Artificially Thickened Wind Tunnel Boundary Layers," Report LTR-LA-37, N.A.E., (1969).

9. Davenport, A.G., "The Relationship of Wind Structure to Wind Loading," Paper No. 2, Symp. 16, Procedures of Conference on Buildings and Structures at NPL, June 1963, HMSO, London (1965).

10. Prandtl, L., "Uber Flussigkeitsgewegung bei sehr kleiner Reibung," Proc. 3rd Intern. Math. Congr., Heidelberg, (1904), (English Translation NACA TM 452, 1928).

11. Clauser, F.H., "The Turbulent Boundary Layer," Advances in Applied Mechanics, Vol. 4, (1956).

12. Nikuradse, J., "Stromungesgesetze in rouhen Rohren," VEI - Forschungsheft, No. 361, (1933).

13. Hinze, J.O., Turbulence, McGraw-Hill Inc., 2nd ed. (1975).

14. Antonia, R.A., and Luxton, R.E., "The Response of a Turbulent Boundary Layer to a Step Change in Surface Roughness," Journal of Fluid Mechanics, Vol. 48, (1971), p. 721.

15. Dvorak, F.A., "Calculation of Turbulent Boundary Layers on Rough Surfaces in Pressure Gradient," AIAA Journal, Vol. 7, (1969), p. 1752.

16. Clauser, F.H., "Turbulent Boundary Layers in Adverse Pressure Gradients," Journal of the Aero. Sciences, Vol. 21, (1954), p. 91.

17. Gartshore, I.S., "A Relationship Between Roughness Geometry and Velocity Profile Shape for Turbulent Boundary Layers," Report LTR-LA-140, N.A.E., (October 1973).

18. Engineering Sciences Data Unit, Item 70015, "Fluid Forces and Moments on Flat Plates," (October 1972). Item 71016, "Fluid Forces, Pressures and Moments on Rectangular Blocks," (July 1963).

19. Gartshore, I.S., and de Croos, K.A., "Roughness Element Geometry Required for Wind Tunnel Simulations of the Atmospheric Wind." To be published by A.S.M.E. (preprint 76-WA/FE-18).

20. Mellor, G.L., and Gibson, D.M., "Equilibrium Turbulent Boundary Layers," "Journal of Fluid Mechanics, Vol.24, (1966), p. 255.

21. Townsend, A.A., The Structure of Turbulent Shear Flow, Cambridge University Press, 2nd ed., (1956).

22. Perry, A.E., Schofield, W.H., and Joubert, P.N., "Rough Wall Turbulent Boundary Layers," Journal of Fluid Mechanics, Vol. 37, (1969), p.383.

23. Rotta, J.C., "Progress in Aero Sciences," Vol.2 (ed. Ferri, Kuchemann and Sterne), Pergammon Press, N.Y., (1962)

24. Antonia, R.A., and Luxton, R.E., "The Response of a Turbulent Boundary Layer to an Upstanding Step Change in Surface Roughness," ASME, Paper No. 70-FE-1, (May 1970). Delivered at Fluids Engineering, Heat Transfer and Lubrication Conference, Detroit, Michigan.

25. Counihan, J., "Wind Tunnel Determination of the Roughness Length as a Function of the Fetch and the Roughness Density of Three-Dimensional Roughness Elements," Atmospheric Environment, Vol. 5, (1971), p. 637.

26. Wooding, R.A., Bradley, E.F., and Marshall, J.K., "Drag Due to Regular Arrays of Roughness Elements of Varying Geometry," Boundary-Layer Meteorology, Vol. 5, (1973), p. 285.

27. Patel, R.P., "Reynolds Stresses in Fully Developed Turbulent Flow in a Circular Pipe," McGill Univ. Report, No. 68-7, (1968).

28. Cowdrey, C.F., "A Simple Method for the Design of Wind Tunnel Velocity Profile Grids," Nat. Physical Lab, Aero Note 1055, (May 1967).

29. Champagne, F.H., "Turbulence Measurements with Inclined Hot Wires," B.S.R.L. Flight Sciences Lab Report, No. 103, (1965).

30. Van der Hoven, I., "Power Spectrum of Horizontal Wind Speed in the Frequency Range from 0.0007 to 900 Cycles per Hour," Journal of Meterology, Vol. 14, (1957), pp. 160-164.

31. Davenport, A.G., "The Dependence of Wind Loads on Meterological Parameters," Paper No. 2, Proceedings of the International Seminar on Wind Effects on Buildings and Structures, National Research Council, Ottawa, (September 1967), pp. 11-15.

32. Templin, R.J., "Interim Progress Note on Simulation of Earth's Surface Winds by Artificially Thickened Wind Tunnel Boundary Layers," Report LTR-LA-22, N.A.E., (February 1969).

APPENDIX 1

Head's empirical functions can be numerically defined[15] as follows:

$$F(H_1) = \exp\left(-3.512 - 0.617 \ln (H_1 - 3)\right)$$

where

$$H_1 = (\delta - \delta^*) / \theta$$

$$G(H) = 3.3 + \exp\left(.4667 - 2.722 \ln(H - .6798)\right)$$

for $H \leq 1.6$

$$G(H) = 3.3 + \exp\left(.4383 - 3.064 \ln(H - .6798)\right)$$

for $H > 1.6$

where

$$H = \delta^*/\theta \quad .$$

APPENDIX 2

The slanted hot wire anemometer technique for measuring shear stress used by Patel follows the work of Champagne[29] and others. Basically, the technique uses two readings of the hot wire rms voltage ($\bar{e}^2$). The slant wire is set at an angle $+\psi$ into the mean wind direction and the first set of rms readings ($\bar{e}_1^2$), taken. Now the slant wire is turned 180° in the plane defined by the wire and mean wind velocity, to an angle $-\psi$, and the second set of readings taken.

The shear stress is given as

$$\frac{\tau}{\rho U_1^2} = \frac{\left(\frac{\bar{e}_1^2}{E_1^2} - \frac{\bar{e}_1^2}{E_2^2}\right)}{4} \left[\frac{1 + k_1^2 \cot^2 \psi}{(1 - k_1^2)\cot^2 \psi}\right]$$

where e, E are the rms and mean voltage readings taken by the slant wire at each orientation respectively.

Usually, $\psi = 45°$ and $k_1 = 0.2$, so that the equation above reduces to

$$\frac{\tau}{\rho U_1^2} = \left(\frac{U_\tau}{U_1}\right)^2 = 0.27 \left(\frac{\bar{e}_1^2}{E_1^2} - \frac{\bar{e}_2^2}{E_2^2}\right) .$$

TABLE I

Dimensions of Modified Half-Width Spires

Height (in)	Spire Width (in)
0.0	16.00
0.5	8.80
2.5	6.30
5.0	4.95
7.5	4.05
10.0	3.35
15.0	2.25
20.0	1.35
24.0	0.00

TABLE II

Variation of the Defect Law Integral Parameter and von Karman's Constant with Distance Downstream for the Naturally Grown Boundary Layer

$\frac{x}{k}$	$\frac{U_1 \delta^*}{U_\tau \delta}$	K
140.8	4.26	0.33
268.8	4.24	0.35
332.8	4.13	0.38
396.8	3.99	0.38
492.8	3.96	0.34

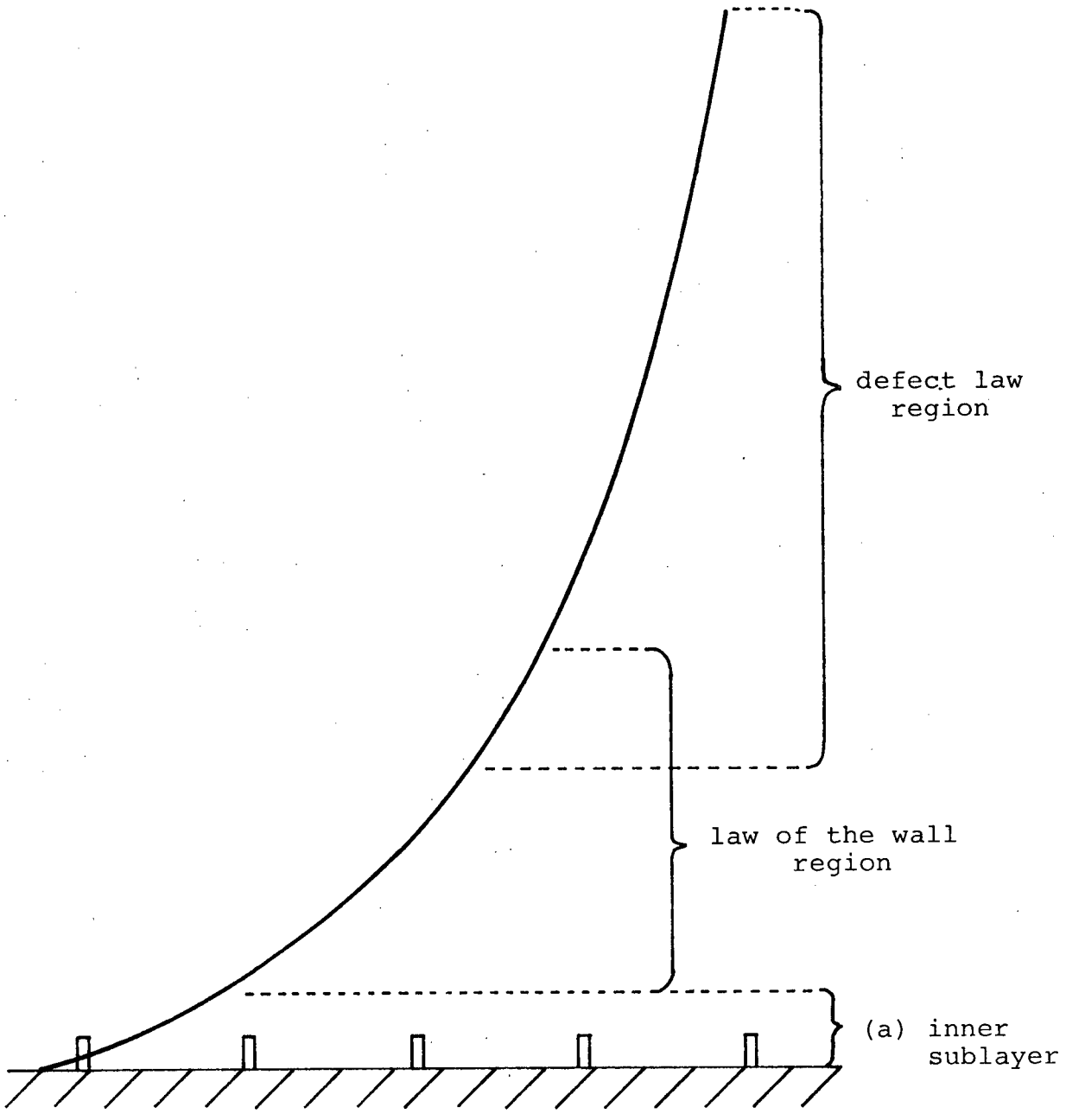

Figure I Structure of the rough wall boundary layer

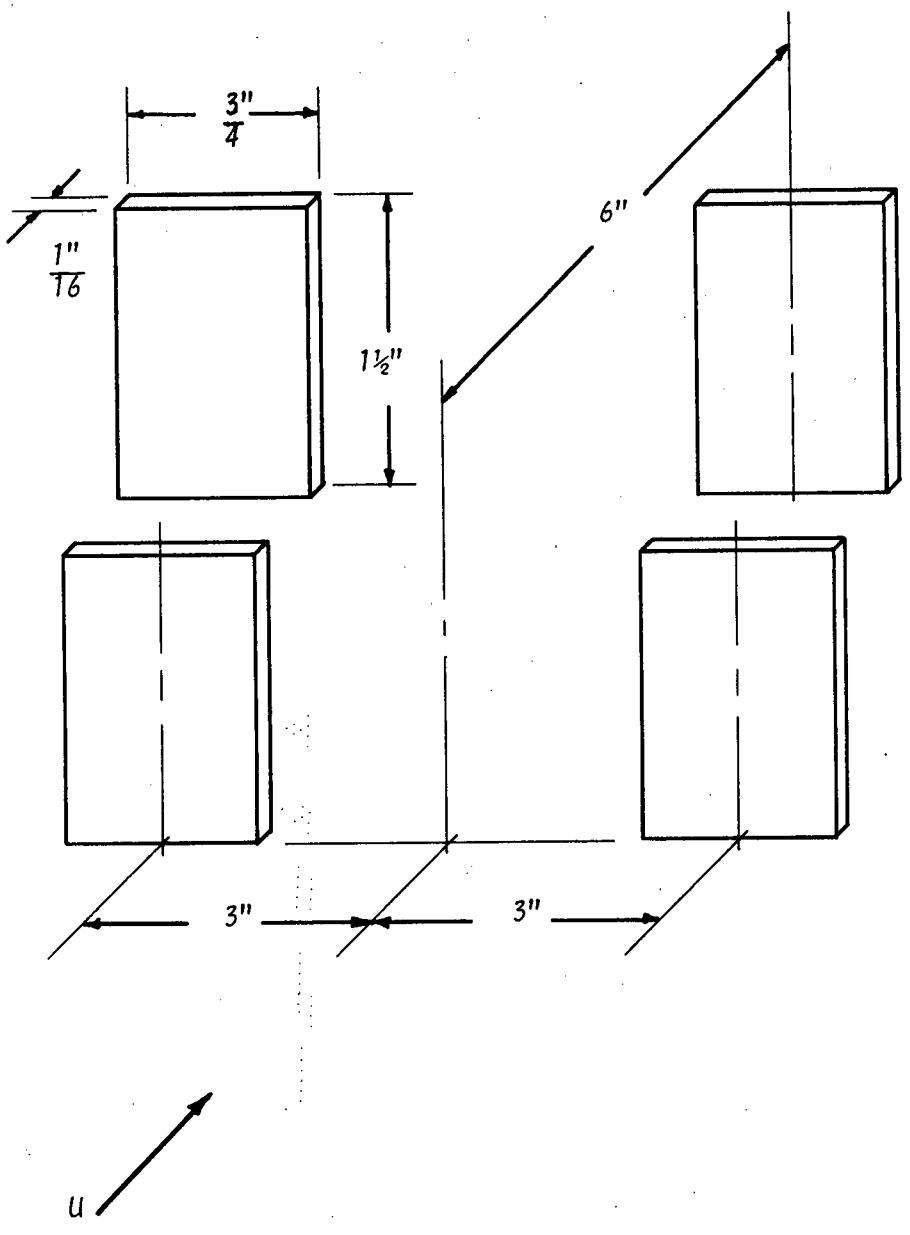

Figure 11 Roughness element spacing and dimensions

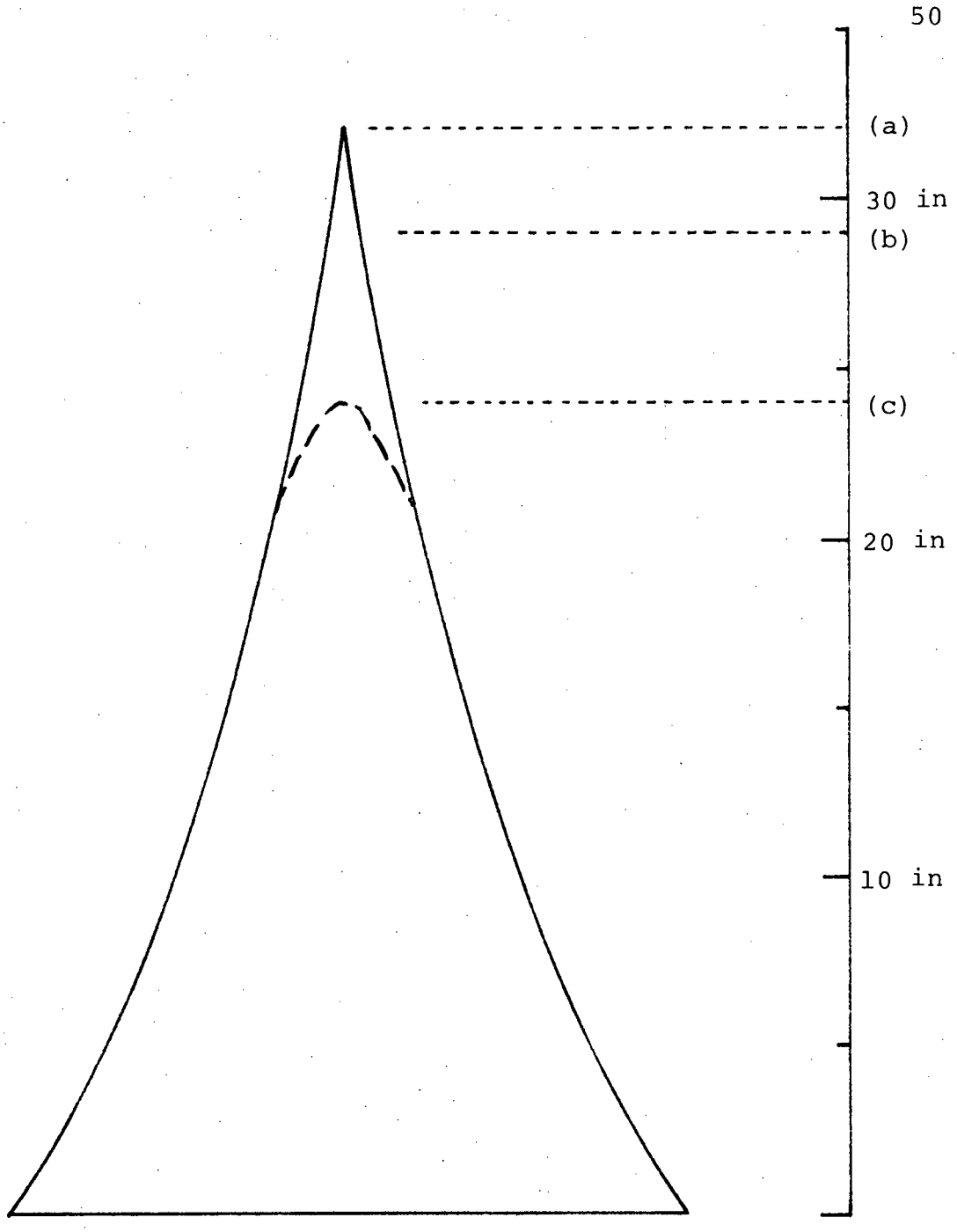

— — — actual spires

——— design of spires

(a) design spire height (32 in)

(b) boundary layer thickness (29 in)

(c) actual spire height (24 in)

Figure III Spire dimensions

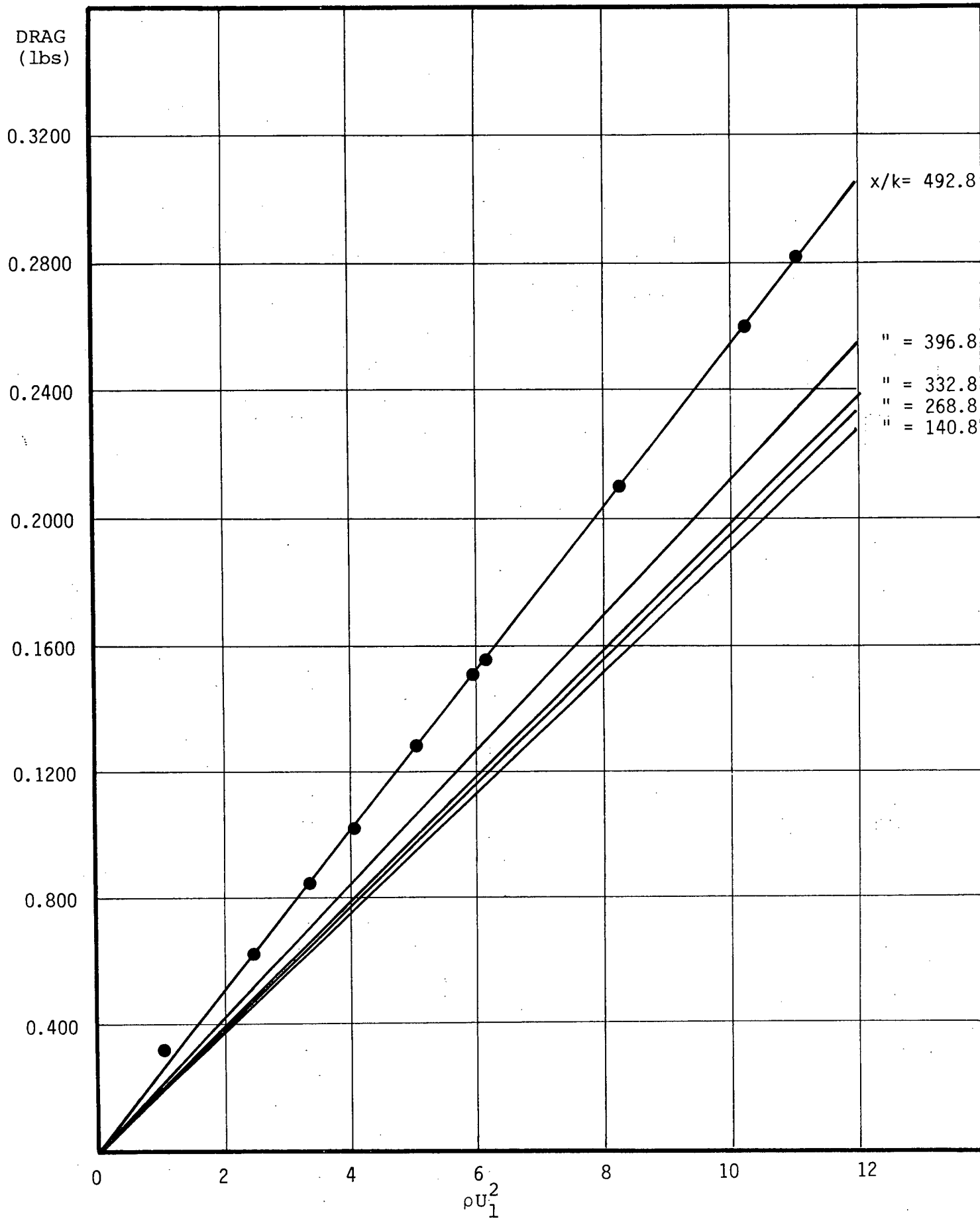

Figure IV Drag vs. ρU_1^2; naturally grown boundary layer

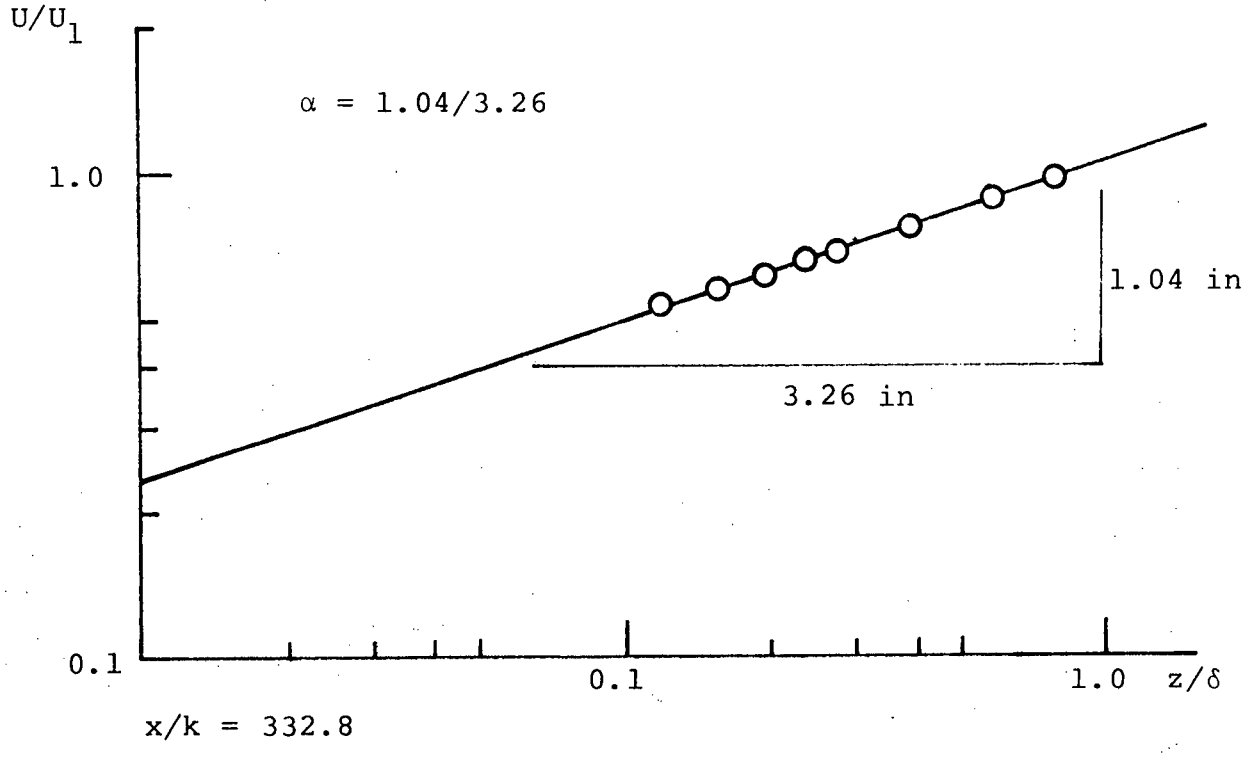

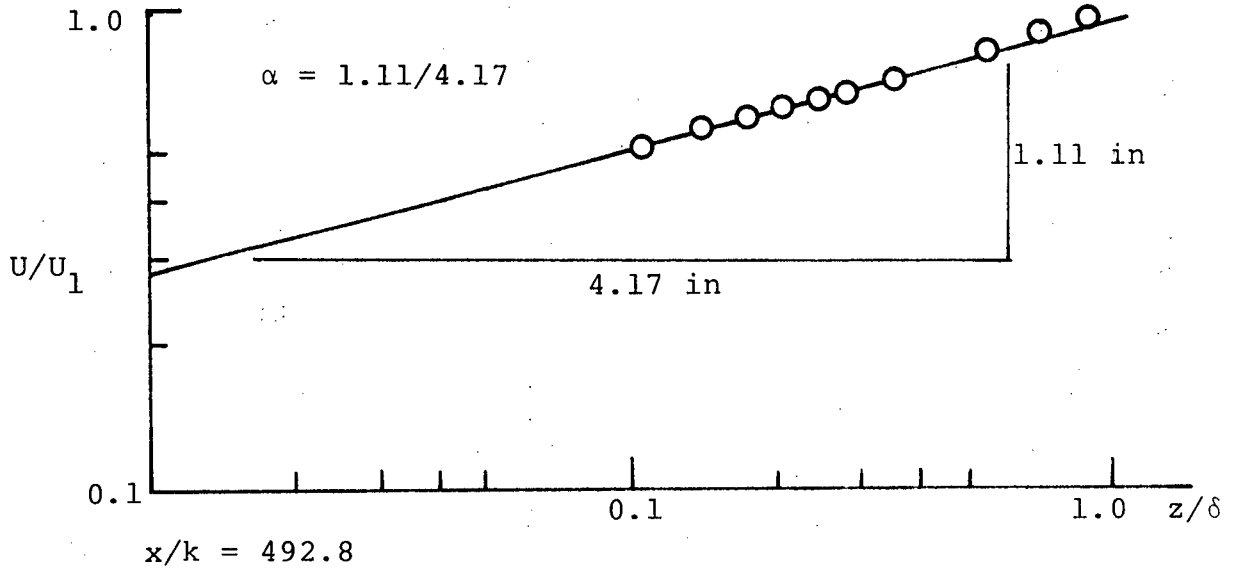

Figure V Sample log-log velocity profiles

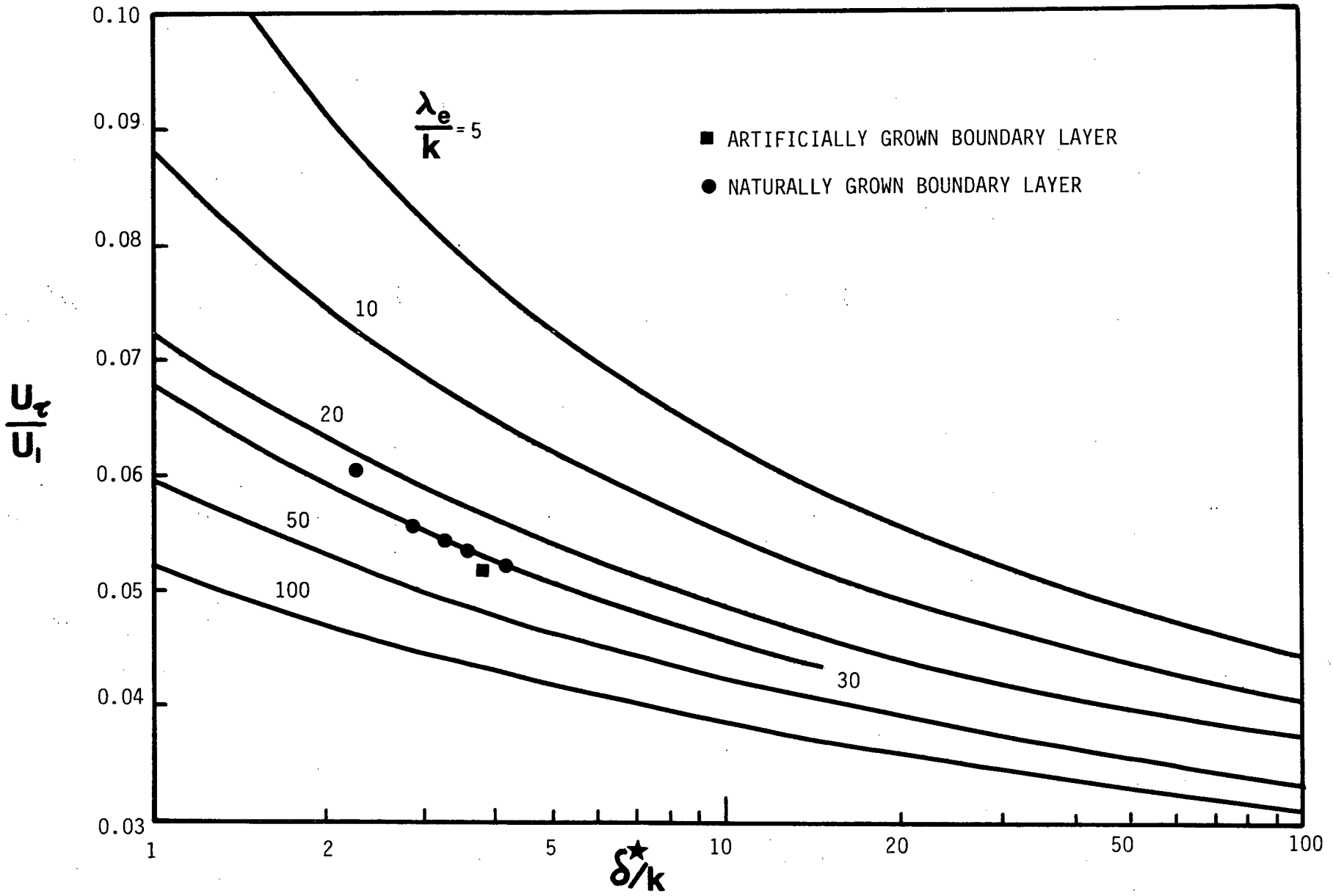

Figure VI Wall shear stress expected for various roughness geometries (Dvorak's correlation)

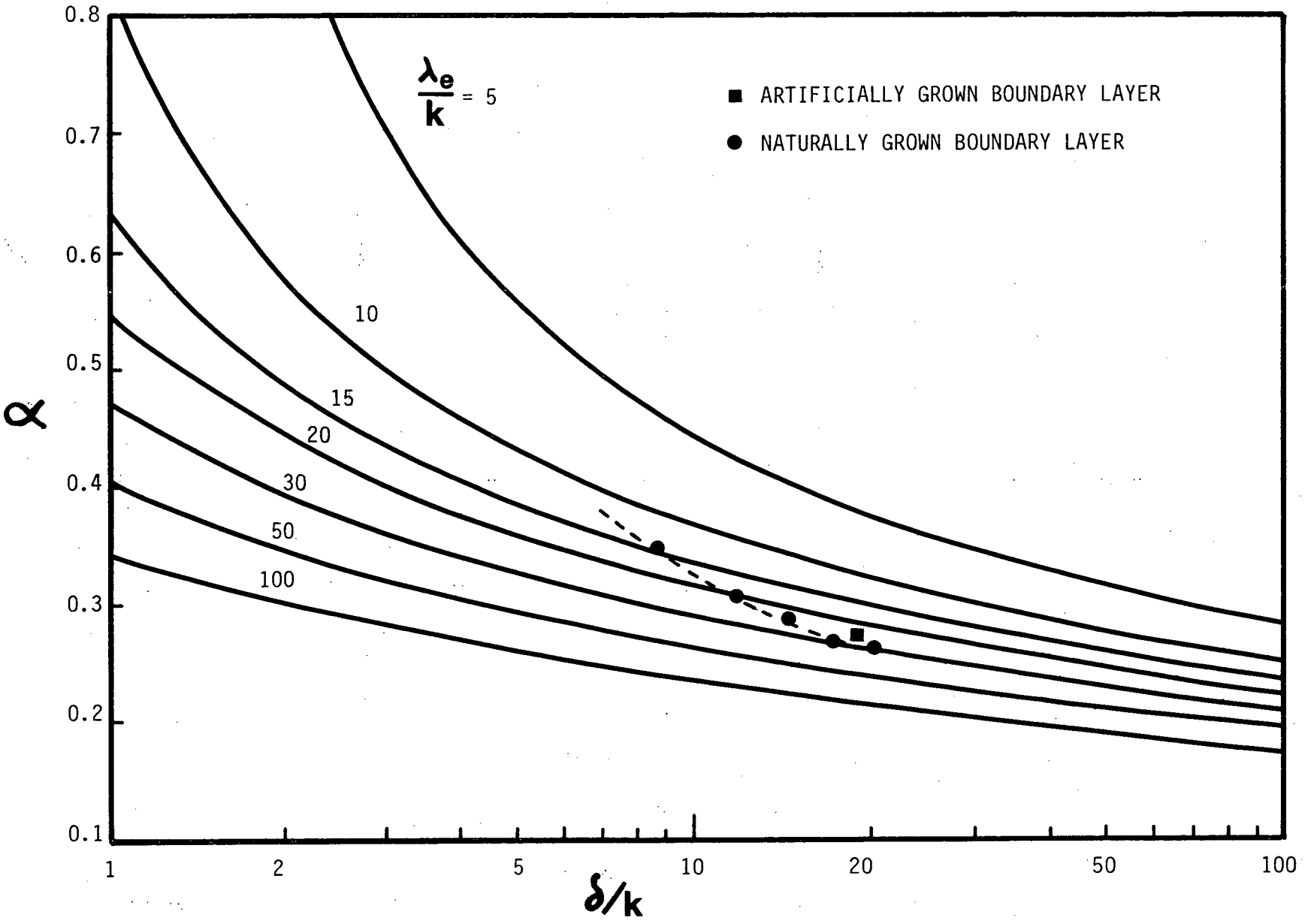

Figure VII Effect of roughness geometry on profile shape (Dvorak's correlation)

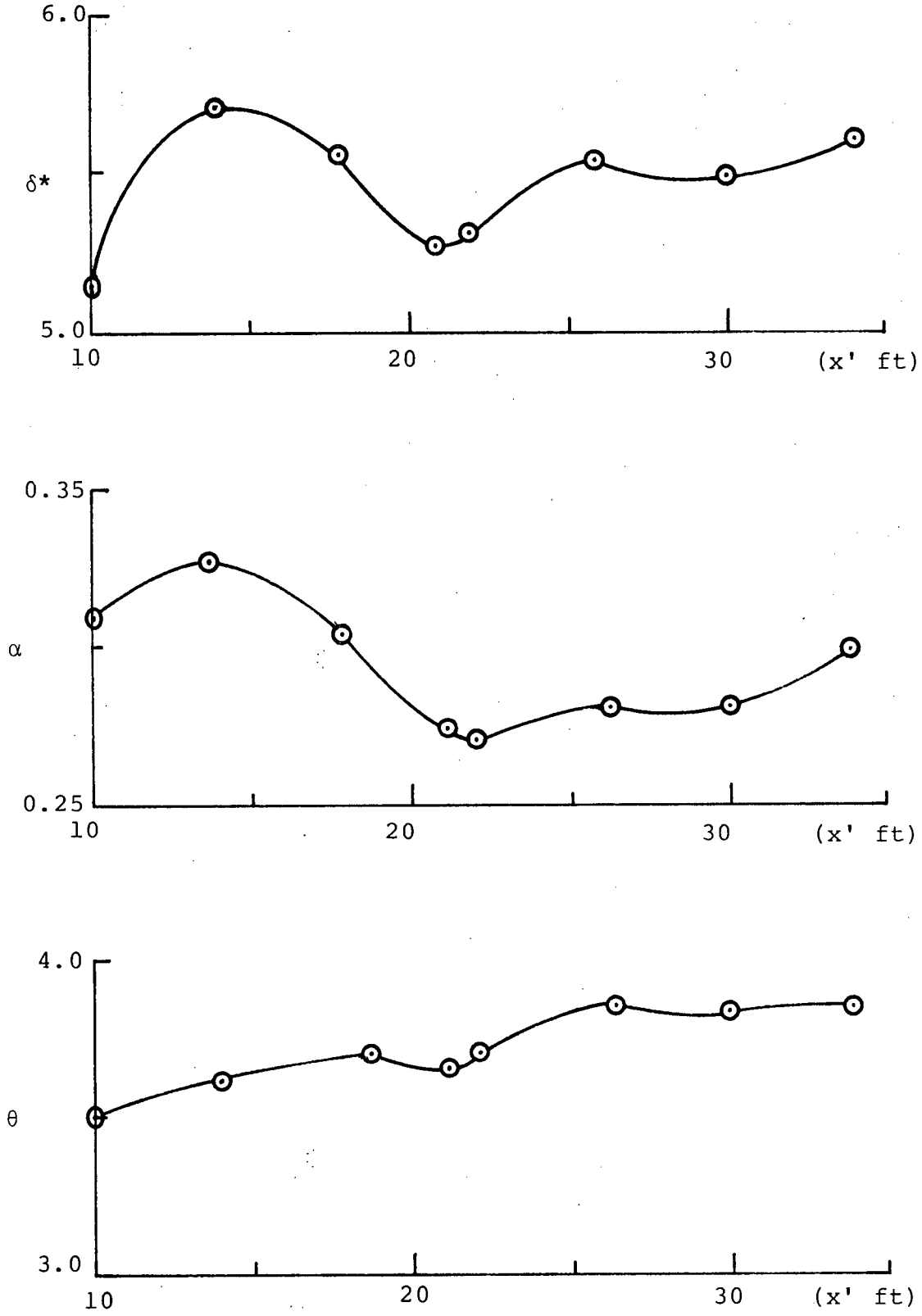

Figure VIII Variation of gross characteristics δ^*, α and θ with distance behind spires x', for the artificially grown boundary layer

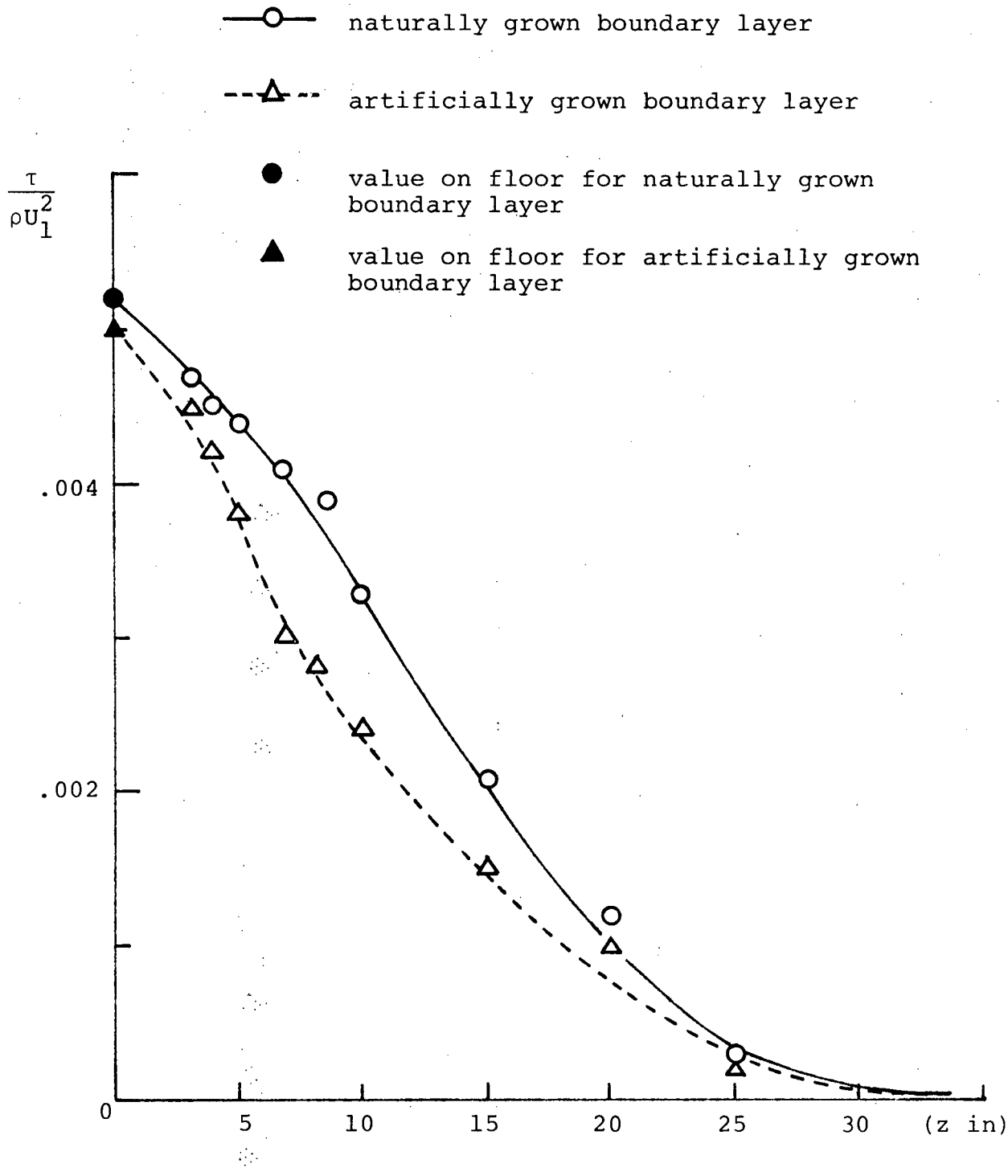

Figure IX Shear stress as measured using a slant wire

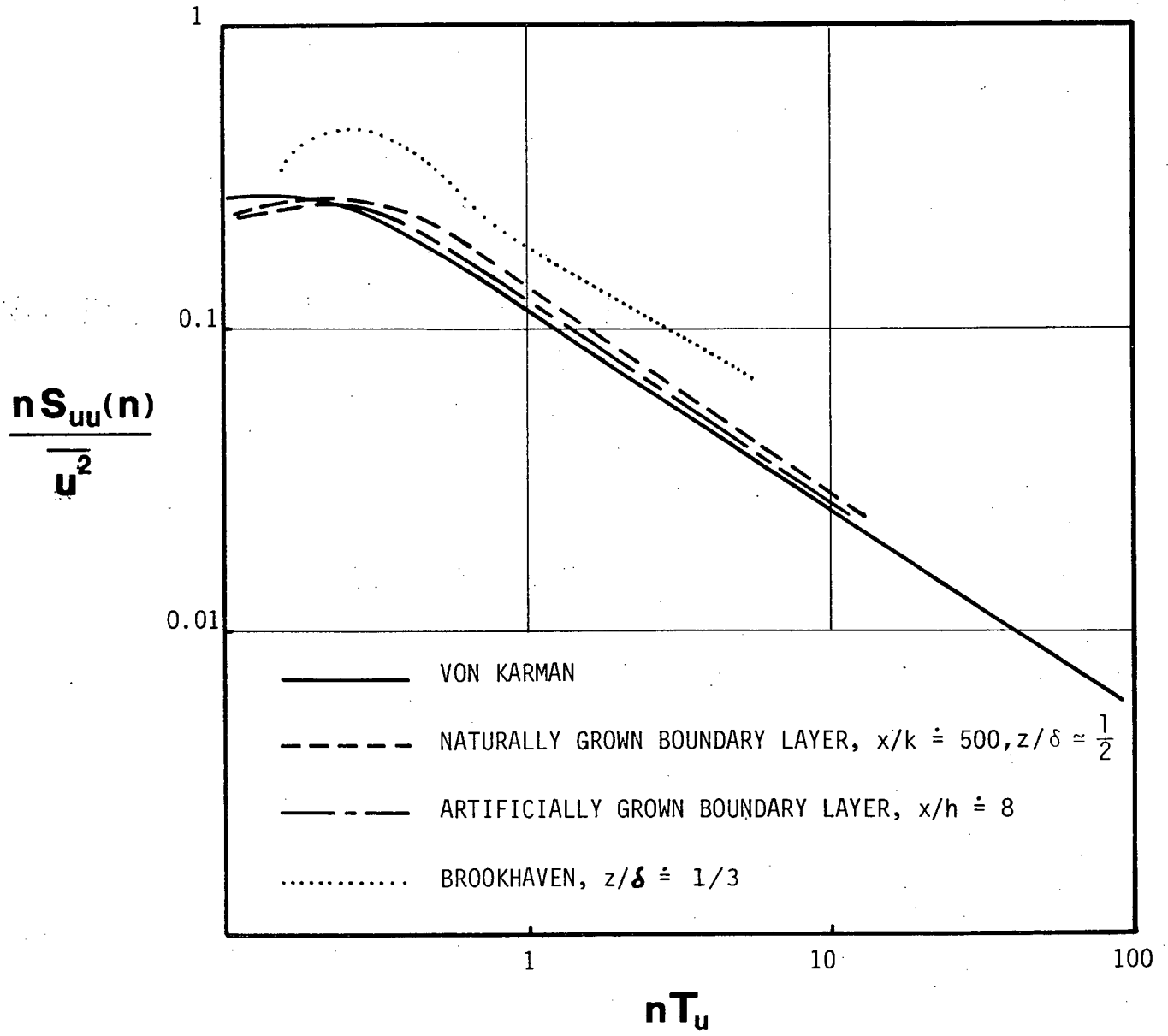

Figure X Power spectral density of the longitudinal turbulence - Height 15" above the floor

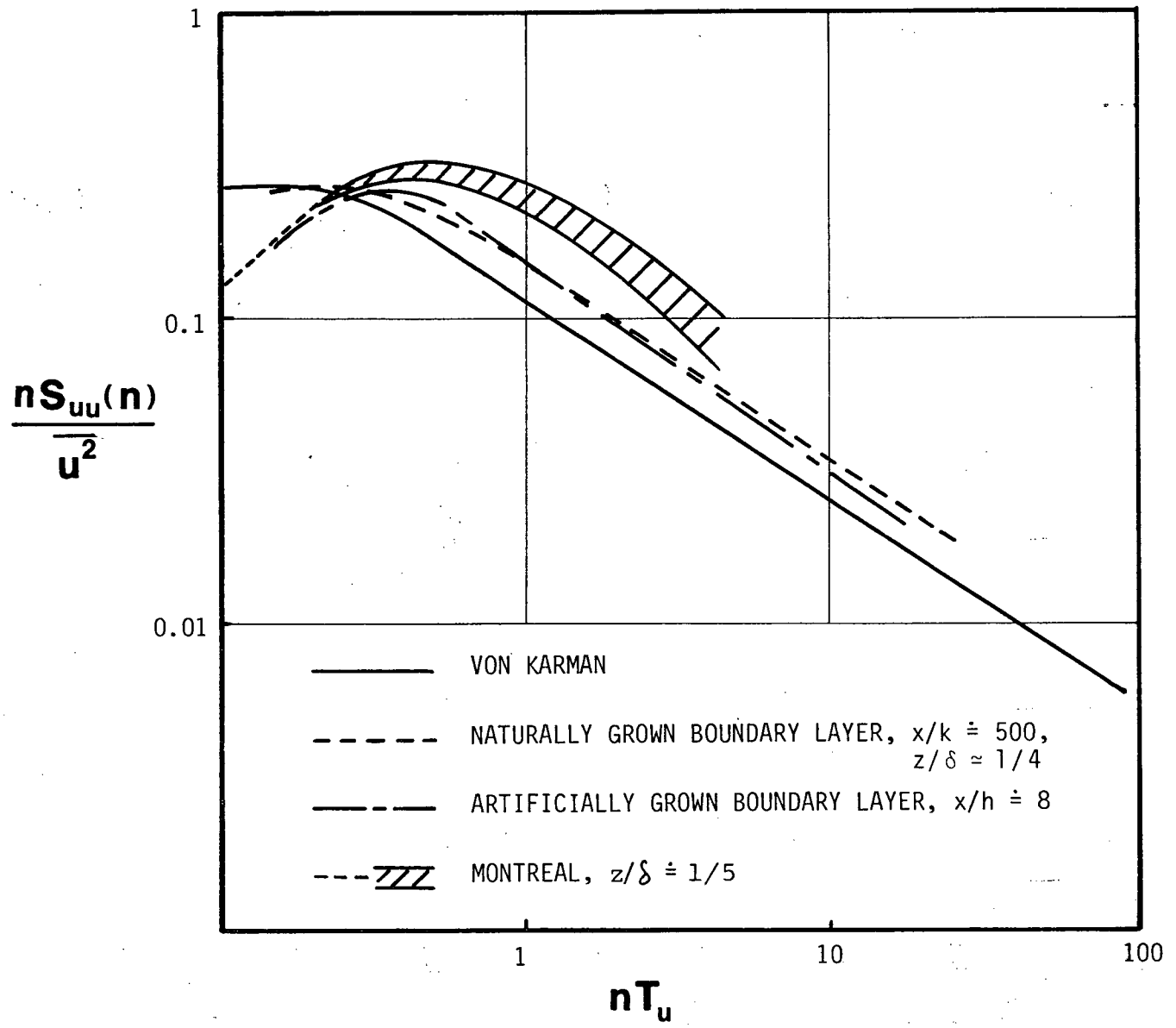

Figure XI Power spectral density of the longitudinal turbulence - Height 8" above the floor

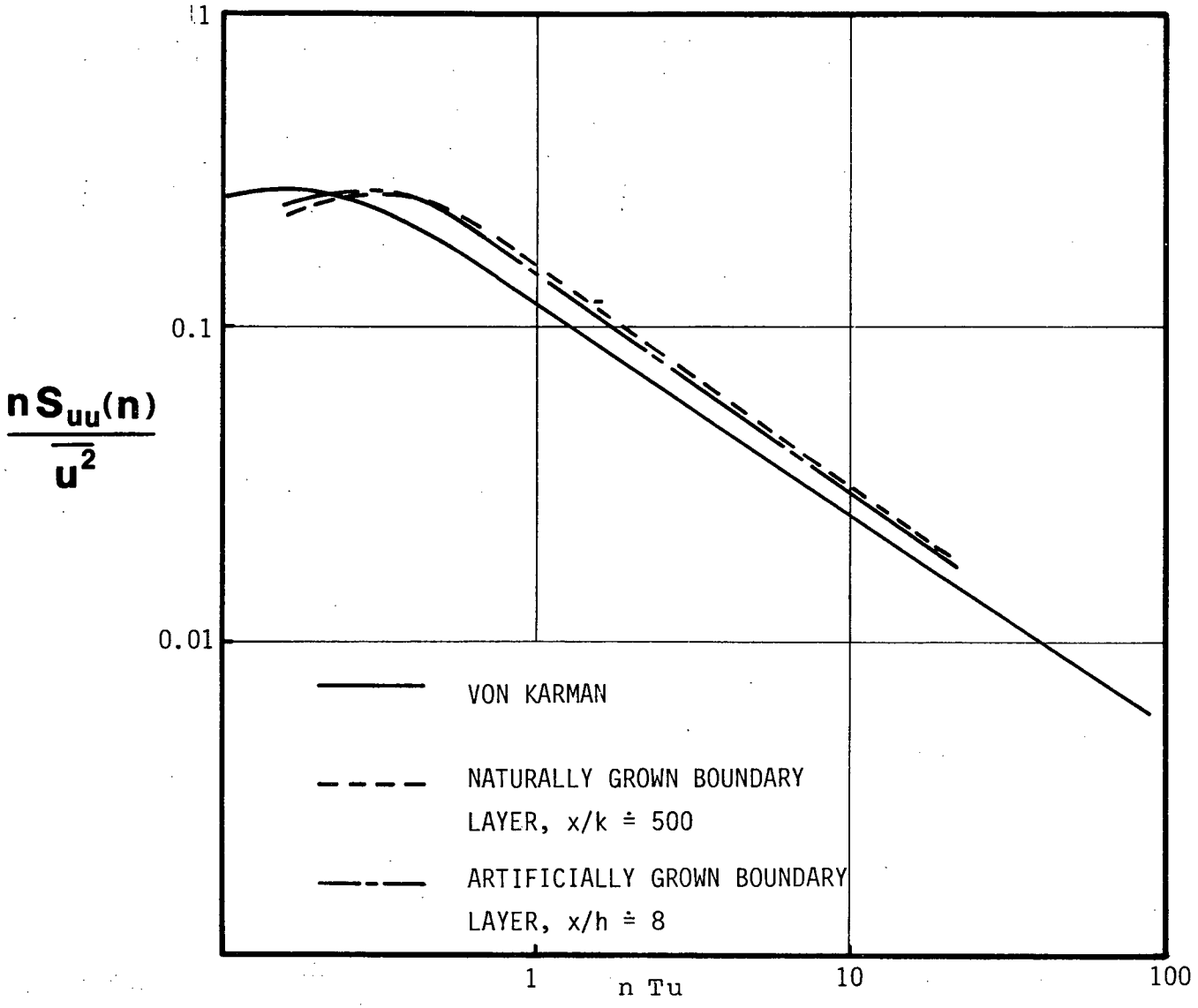

Figure XII Power spectral density of the longitudinal turbulence - Height 3" above the floor

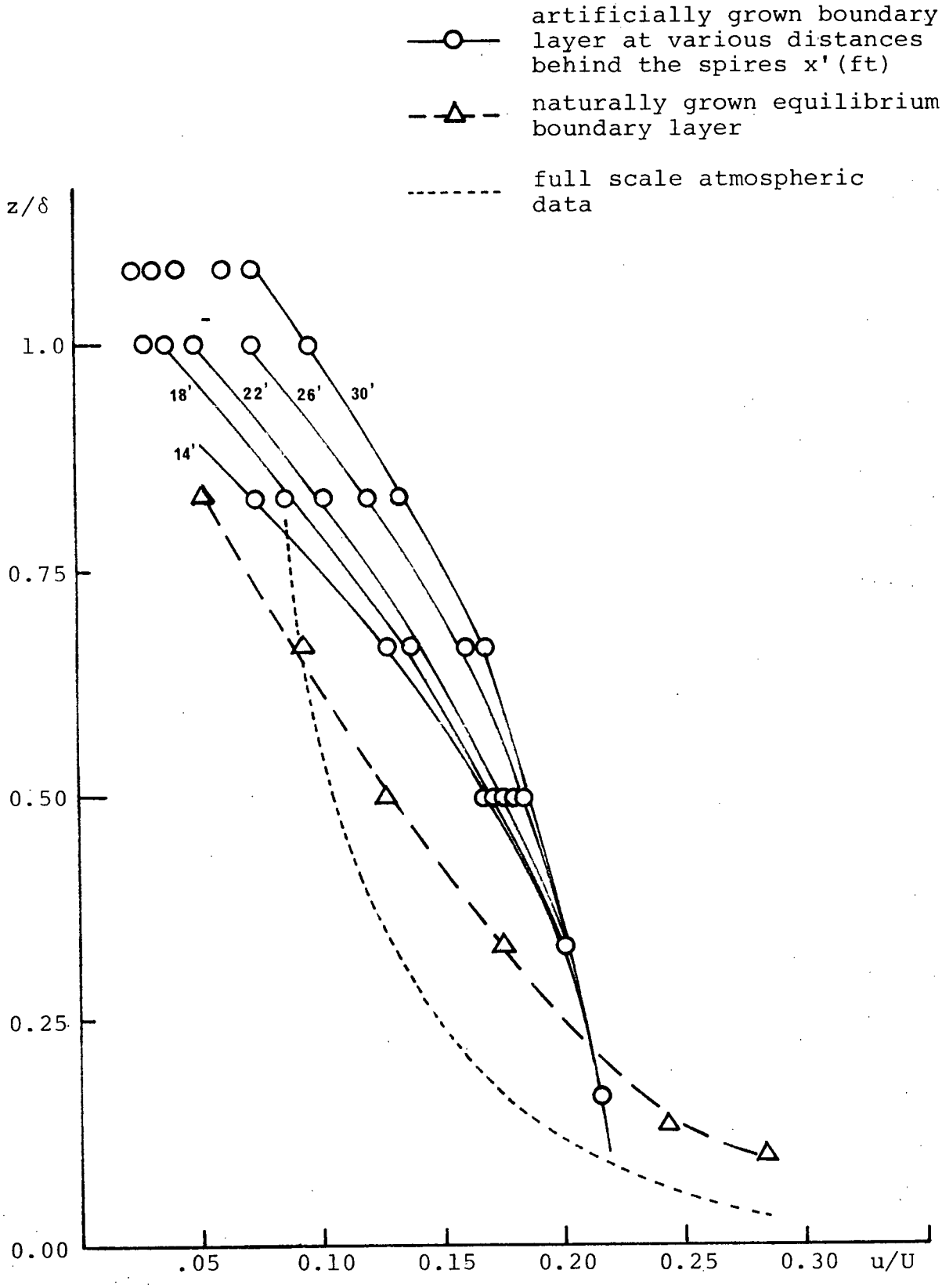

Figure XIII Longitudinal turbulence intensity